

Automated Two-Axes Optical Fiber Alignment Using Grayscale Technology

Brian Morgan, *Member, IEEE*, Jonathan McGee, *Student Member, IEEE*, and Reza Ghodssi, *Member, IEEE*

Abstract—In this paper, we report a new method for actuating an optical fiber in two axes. This device enables in package active alignment of an optical fiber towards reducing the time and cost of optoelectronic packaging by eliminating the need for expensive and slow macroalignment machines. Opposing comb-drive actuators with integrated three-dimensional (3-D) wedges (fabricated using grayscale technology) create a dynamic v-groove to alter the horizontal and vertical alignment of an optical fiber cantilever. All structural components are fabricated in silicon using a single lithography and dry-etching step, making the system conducive to batch fabrication, an essential element to minimize the cost of including in-package alignment capabilities. Actuation of a cleaved fiber tip greater than $30\ \mu\text{m}$ in each direction is demonstrated, with automated fiber alignment times on the order of 10 s, comparable to those achieved using macroalignment systems. Alignment tolerances are held below $1.25\ \mu\text{m}$ over a $20\text{-by-}20\text{-}\mu\text{m}$ actuation area for the first time. The influences of alignment target location, actuation parameters, and alignment algorithm on total alignment time are also presented. [2006-0123]

Index Terms—Comb-drive actuators, fiber alignment, grayscale technology.

I. INTRODUCTION

ALIGNMENT of an optical fiber within an optoelectronic module is a continuing challenge in photonics packaging and often dominates module cost. Ultimately, passive alignment and packaging techniques would be preferred for their simplicity. Passive systems utilizing silicon waferboards have reported alignment accuracies of $1\text{--}2\ \mu\text{m}$ [1], yet this accuracy is achieved by increasing process controls. These tight fabrication and assembly tolerances complicate fabrication and increase the demands on pick-and-place machines, severely limiting throughput. Relaxing placement tolerances from the $1\text{-}\mu\text{m}$ level to $20\text{-}\mu\text{m}$ level could potentially increase throughput of a pick-and-place machine by an order of magnitude [2], but a mechanism for optimizing alignment within the package is then required. In addition, current alignment requirements are approaching $0.2\ \mu\text{m}$ in many applications [3], making passive alignment unrealistic, regardless of the amount

of process control. Thus, to alleviate the need for expensive and slow macroactuators currently required to achieve submicron alignment, multiaxis in-package methods for final alignment of the optical fiber are attractive.

The primary challenge for in-package alignment systems is realizing both horizontal and vertical actuations of the fiber to compensate for shifts of the optical axis in either direction. Previous fiber actuators in microelectromechanical systems (MEMS) have demonstrated multiaxis fiber actuation [4], [5]. However, these systems typically require complicated fabrication (LIGA, a German acronym for X-ray lithography, electroplating, and molding, [4]) and/or specialized fiber preparation (attachment of permanent magnets to the fiber tip [5]) which limit their feasibility as a packaging option. In contrast, the two-axes fiber actuator developed in this paper requires no significant fiber preparation and is realized using a single lithography and dry-etch step and release. Such an actuator is attractive because it can provide fast, accurate active alignment of optical fibers to edge-coupled optoelectronic devices in a configuration conducive to batch fabrication.

This paper presents the design, fabrication, and characterization of the *grayscale fiber aligner*, demonstrating its value as an automated in-package alignment tool. The alignment range, resolution, and speed achievable using our current device layout are presented. The influences of alignment target location, actuation parameters, and alignment algorithm on total alignment time are also evaluated. Section II of this paper describes the actuator design and principle of operation. Section III discusses the required fabrication steps, in particular the use of grayscale technology to integrate the three-dimensional (3-D) wedge structures within electrostatic actuators. Section IV presents both static testing results and automated alignment characterization with regards to speed and accuracy. Some discussion on device improvement is provided in Section V, while concluding remarks are made in Section VI.

II. DESIGN

The *grayscale fiber aligner* exploits the coupled motion of opposing in-plane actuators with integrated 3-D wedges (fabricated using grayscale technology [6]–[8]). Essentially, it creates a dynamic v-groove (controlled via MEMS in-plane actuators) to modify the horizontal and vertical position of the optical fiber [9], [10], as shown in Fig. 1. A top view schematic of the two-axes grayscale fiber aligner is shown in Fig. 2, illustrating its three primary components: a static trench, set of opposing sloped alignment wedges, and in-plane MEMS actuators.

The static trench provides approximate passive alignment of a fiber cantilever similar to an anisotropic v-groove, such that the

Manuscript received June 27, 2006; revised September 15, 2006. This work was supported in part by the U.S. Army Research Laboratory Collaborative Technology Alliance, Power and Energy Consortium under Grant DAAD19-01-2-0010 and by the NASA-Goddard Space Flight Center under Grant APRA04-0000-0087 and the work of R. Ghodssi was supported by the NSF-CAREER Award. Subject Editor S. Merlo.

The authors are with the Department of Electrical and Computer Engineering and the Institute for Systems Research, the University of Maryland, College Park, MD 20742 USA (e-mail: ghodssi@eng.umd.edu).

Color versions of one or more of the figures in this paper are available online at <http://ieeexplore.ieee.org>.

Digital Object Identifier 10.1109/JMEMS.2006.886035

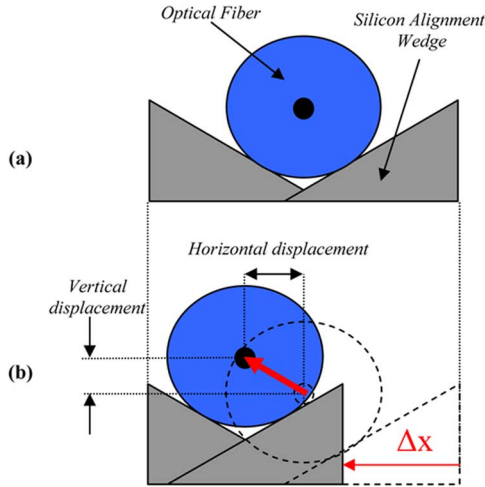


Fig. 1. Optical fiber (a) at rest and (b) after actuating a single wedge, causing horizontal and vertical displacement of the fiber [9].

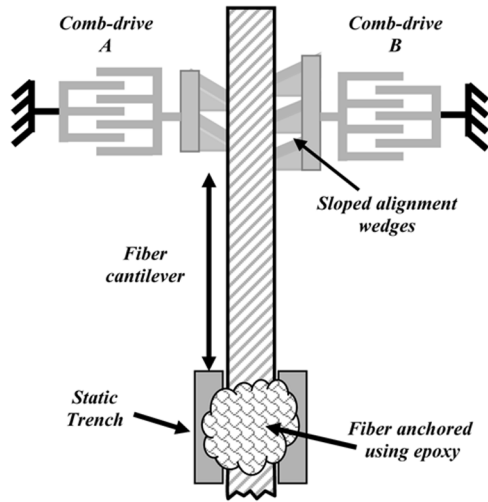


Fig. 2. Top view schematic of the two-axes optical fiber actuator.

fiber's free end rests between the sloped alignment wedges. The anchor point of the fiber determines the length and, therefore, spring constant of the optical fiber cantilever. For example, a 10-mm cantilever results in $k_{\text{fiber}} = 2.5 \text{ N/m}$ according to [11]

$$k_{\text{fiber}} = \frac{3\pi E r^4}{4l^3} \quad (1)$$

where E is Young's modulus of the fiber (silica $\sim 70 \text{ GPa}$), r is the radius of the fiber (typically $62.5 \mu\text{m}$), and l is the length of the fiber cantilever.

The spring constant of the optical fiber must be considered jointly with the mechanics of the in-plane MEMS actuator. For this device, electrostatic comb-drive actuators were selected due to their well-characterized behavior, simplifying both design and control. The force generated by a comb-drive can be modeled analytically using [12]

$$F = N \frac{\varepsilon_0 h}{d} V^2 \quad (2)$$

where N is the number of comb fingers, ε_0 is the permittivity of free space, h is the comb-finger height, d is the gap between

fingers, and V is the applied voltage. Making basic assumptions ($N = 100$, $h = 100 \mu\text{m}$, $d = 10 \mu\text{m}$, and $V = 100 \text{ V}$), we can estimate a generated force in the range of $89 \mu\text{N}$. If this force were applied directly to the fiber cantilever discussed previously, the expected deflection would be $> 35 \mu\text{m}$ ($F = kx$). However, one must also consider two additional factors present in this device. First, the spring constant of the comb-drive suspension will reduce the amount of force directed to the fiber. Second, the sloped wedges push the fiber at an angle, causing the magnitude of fiber deflection to be smaller than the comb-drive deflection. Considering these facts, it is still reasonable to expect fiber actuation on the order of tens of micrometers using comb-drive voltages around 100–150 V on fiber cantilevers in the range of 10–12 mm long.

While these devices may appear large, cantilevers using reduced cladding fiber ($r = 40 \mu\text{m}$) would be more flexible, enabling the cantilever length to be decreased. Similarly, higher force actuators (such as thermal actuators [13]) would allow shorter cantilevers to be used. However, as the cantilever length decreases, the angle created by bending the fiber a certain distance increases, countering the improvement in coupling achieved by reducing axial misalignment. We can see these competing trends when we calculate the transmission between two cleaved, single-mode fibers. The transmission (T) as a function of axial and angular misalignment can be written as [14]

$$T = \left(\frac{2\omega_1\omega_2}{\omega_1^2 + \omega_2^2} \right)^2 \exp \left[\frac{-2d^2}{(\omega_1^2 + \omega_2^2)} \right] \quad (\text{axial}) \quad (3)$$

$$T = \left(\frac{2\omega_1\omega_2}{\omega_1^2 + \omega_2^2} \right)^2 \exp \left[\frac{-2(\pi n_2 \omega_1 \omega_2 \theta)^2}{(\omega_1^2 + \omega_2^2) \lambda^2} \right] \quad (\text{angular}) \quad (4)$$

where ω_1 and ω_2 are the mode field width of each fiber, n_2 is the refractive index of the second fiber, λ is the wavelength of light being considered, d is the axial misalignment between fibers, and θ is the angular misalignment between fibers. Using $9\text{-}\mu\text{m}$ core single-mode fibers at 1550 nm , we can calculate the expected loss as a function of both axial and angular misalignment, where the angle is determined by the cantilever length and magnitude of tip deflection. The losses for axial and angular misalignment are plotted in Fig. 3(a) and (b), respectively. (Note that loss due to longitudinal separation of the fiber is much less sensitive to small changes in position [14], making active alignment along that axis unnecessary.) We see that the loss caused by axial misalignment of only a couple of micrometers is far dominant over all the angular cases shown. However, as the cantilever gets shorter, the angular misalignment loss from bending the fiber could become significant. For current devices, this is not a concern because fiber cantilever lengths were kept $\geq 10 \text{ mm}$, but these calculations underscore the fact that the mechanical and optical design limitations must be considered jointly.

The most critical components of this fiber actuator are the opposing sloped alignment wedges, since they contact the fiber directly and enable the out-of-plane actuation. The emerging 3-D silicon fabrication technique, *grayscale technology* [6]–[8], was selected to fabricate the required 3-D silicon wedges due to its ability to batch fabricate arbitrary 3-D features in silicon.

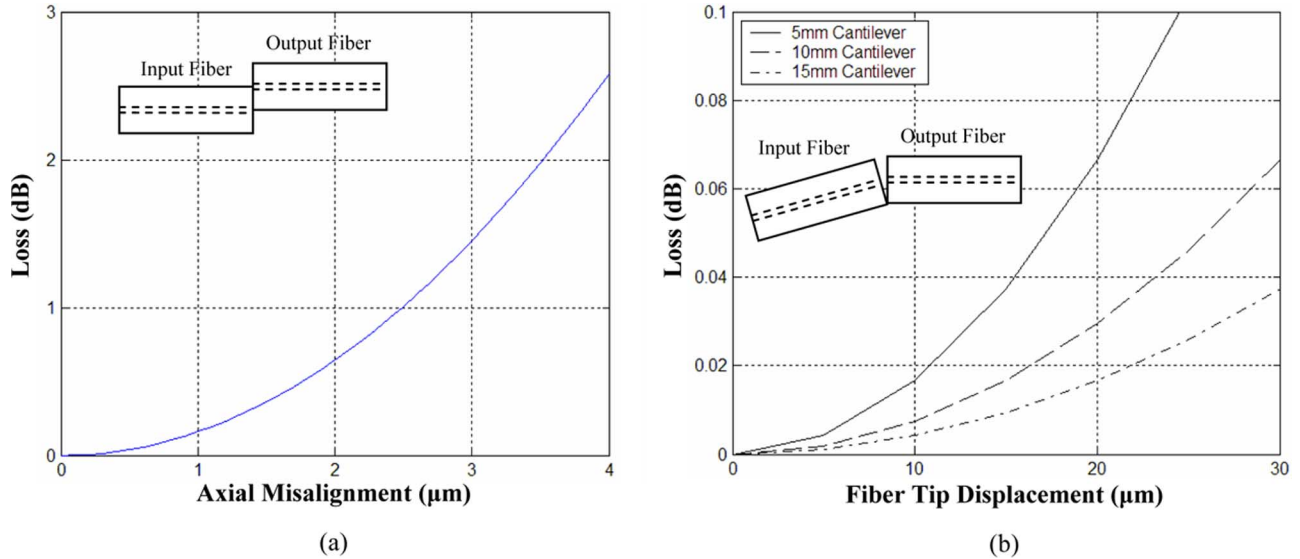


Fig. 3. Modeled coupling loss between identical single-mode fibers that have either (a) purely axial misalignment or (b) purely angular misalignment. The angle created by bending the fiber is a function of both the fiber cantilever length and displacement at the tip.

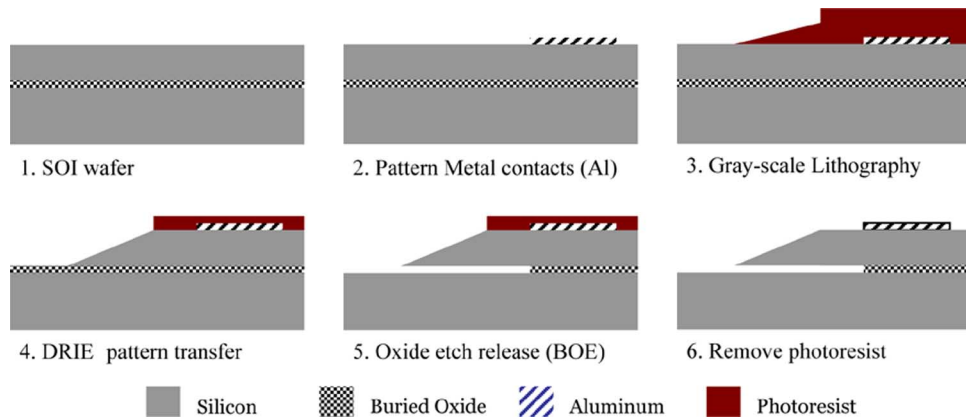


Fig. 4. Process flow for creating electrostatic MEMS actuators with integrated 3-D components [15].

Grayscale technology uses a single variable intensity exposure to create a 3-D photoresist mask that is subsequently transferred into the underlying substrate using deep reactive ion etching (DRIE). The method of grayscale implementation chosen for this paper is based on the pixilated approach described by Waits *et al.* [6], which uses many subresolution opaque pixels in a projection lithography system. Specifically developed DRIE recipes are then used to control the relative etch rate of silicon to photoresist, called “*etch selectivity*,” to define the final vertical dimensions of the 3-D structure in silicon.

The sloped wedges should be smooth compared to the size of the optical fiber ($r = 62.5 \mu\text{m}$) to enable continuous motion. Therefore, a grayscale mask design containing 50 *gray levels* (each a different size pixel on the mask) was created to define the sloped wedges. An angle of 45° was chosen for the wedge design, as shallow or steep angles could cause slippage or jamming of the fiber. Using this wedge angle, one can calculate the “rest” position of a fiber in the dynamic v-groove created by the sloped wedges. From this rest position, shown previously in Fig. 1(a), the following three primary actuation paths are available: 1) moving the left actuator causes motion up and to the

right, 2) moving the right actuator causes motion up and to the left, and 3) moving both actuators equally causes motion straight up. These trajectories form a diamond-shaped alignment area, within which the fiber tip can move given the appropriate combination of voltages.

III. FABRICATION

The grayscale process was first integrated with a silicon-on-insulator (SOI) MEMS comb-drive process flow by our group [15] and is mimicked here (see Fig. 4). A buried oxide layer of $2 \mu\text{m}$ and an SOI device layer of $100 \mu\text{m}$ were used, primarily to match the dimensions of a standard single mode optical fiber (diameter = $125 \mu\text{m}$). Metal liftoff was used to pattern aluminum contact pads and alignment marks. Next, grayscale lithography was performed using the specifically designed grayscale optical mask. DRIE transferred the planar and variable height structures into the silicon simultaneously. The *etch selectivity* was controlled to properly amplify the vertical dimensions of each gray level from photoresist into silicon to achieve the desired wedge angle of approximately 45° . Before removing the remaining photoresist, the wafer was placed in buffered oxide etch (6 : 1)

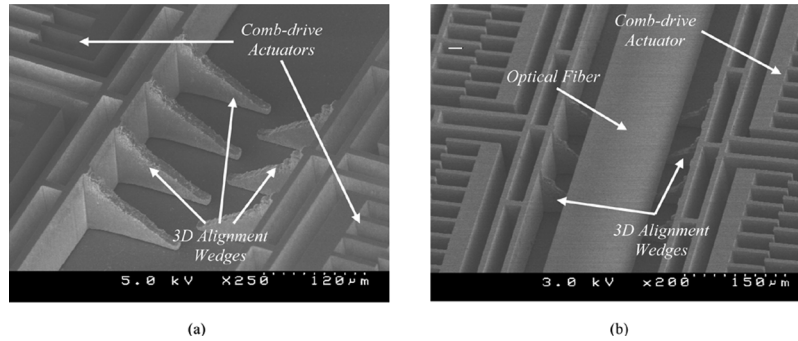


Fig. 5. SEMs of grayscale fiber aligners (a) before and (b) after fiber attachment [10].

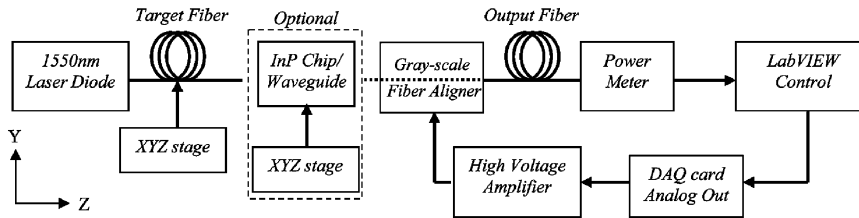


Fig. 6. Optical test setup for autoalignment of MEMS-actuated fiber to other fibers or InP waveguides.

to remove the sacrificial buried oxide layer. Oxygen plasma was used to strip the remaining photoresist to avoid stiction problems with the suspended structures. Fabricated electrostatic actuators with 3-D wedges are shown in the scanning electron micrograph (SEM) of Fig. 5(a). Since quantitative roughness measurements are challenging on such sloped, high aspect ratio structures, SEM inspection was used to estimate a roughness of 1–3 μm over the majority of the slope [10]. It was observed during testing that rougher wedges resulted in fiber motion with large discrete movements and poor actuation precision.

For final assembly, a single-mode optical fiber (Corning SMF-28) was manually stripped and cleaved. The cleaved free end of the fiber was placed between the alignment wedges. The bulk fiber was then secured in the static trench with ultraviolet (UV)-curing epoxy to create a flexible cantilever. The cleaved facet of the fiber hangs slightly off the edge of the SOI chip (< 1 mm) to enable coupling to external devices.

A device after fiber attachment is shown in Fig. 5(b). Since the fiber attachment process is entirely manual, it is difficult to consistently ensure that the fiber touches both wedges in its rest state. Reliable operation can be achieved with small gaps between the wedge and fiber, but requires a voltage offset to move the wedges into contact before the fiber begins to move.

IV. TESTING

A. Test Methodology

The optical setup used to test the grayscale fiber aligner is shown in Fig. 6 [10]. A 1550-nm laser diode and optical power meter are used to assess the coupled power between two optical fibers located on electrostrictively-controlled XYZ stages. LabVIEW was used to control each electrostrictive stage, as well as the actuation voltages for the grayscale fiber aligner (via data acquisition card and high-voltage amplifier). A settling time (pause between discrete fiber movements) of at least

300 ms is necessary to allow sufficient time for the fiber to settle and the power meter to read accurately.

This setup is quite flexible and enables two primary tests to be performed. The first test determines the location of a fixed cleaved tip of the fiber aligner. The calibrated electrostrictive stage is swept in the X - Y plane (perpendicular to light propagation) to map the coupled power as a function of location (a facet scan). The location of peak coupling indicates the location of the fiber core. This first test enables characterization of the movement of the cleaved fiber tip, but is rather time consuming.

The second type of test evaluates autoalignment algorithms for both speed and accuracy, where a target fiber (or waveguide) is fixed and the grayscale fiber aligner maximizes optical coupling. Tests throughout the grayscale fiber aligner's range were performed using either lensed fibers or indium–phosphide (InP) waveguides as the alignment target.

Sections IV-B–IV-D discuss static fiber deflection testing results, as well as automated alignment results focusing on speed and accuracy.

B. Static Testing

To investigate the extents of fiber movement, four voltage combinations were applied to the two actuators while measuring the location of the grayscale fiber aligner tip. These four points shown in Fig. 7 represent the extreme movements of each alignment wedge. Fiber positions within the diamond-shaped bounds of these measurements (37 μm tall, 48 μm wide) should be achievable given the appropriate set of applied voltages. The slight asymmetry of this diamond is attributed to the fabricated wedge angle being closer to 40° instead of 45°, as well as non-linear spring behavior at large actuator deflections ($\sim 50 \mu\text{m}$).

If one wedge is kept stationary and the other moved, the fiber tip should trace out an angled trajectory parallel to one side of the diamond-shaped alignment area shown in Fig. 7. Yet, in some cases it may be advantageous to move the fiber along

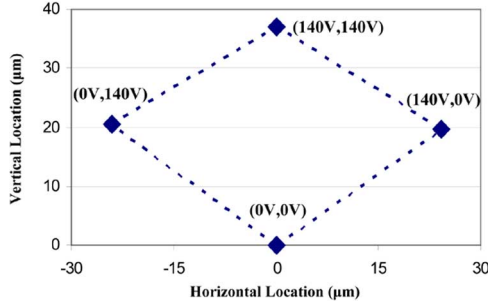


Fig. 7. Measured fiber location for extreme actuation voltages, which form a diamond-shaped alignment area.

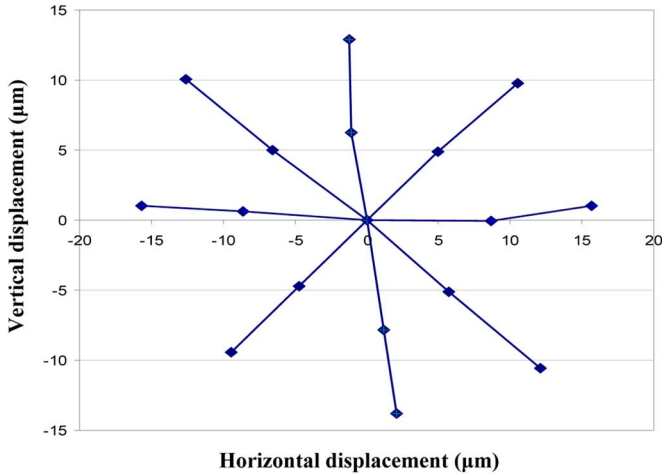


Fig. 8. Primary axes of movements show trajectories every 45° , demonstrating Cartesian control of fiber is possible.

Cartesian coordinates, for example, to simplify mapping of optical sources with asymmetric modes. To make this Cartesian transform, we start by assuming 45° wedges and a set of current voltages (V_A, V_B) applied to the two comb-drive actuators (“A” and “B” from Fig. 2). We then define the desired Cartesian trajectory (U) to be

$$\vec{U} = \alpha \cdot \hat{x} + \beta \cdot \hat{y} \quad (5)$$

where α and β are in units of squared volts because comb-drive force is proportional to the voltage squared. The new set of voltages ($V_{A\text{-new}}, V_{B\text{-new}}$) required to create this trajectory is then

$$V_{A\text{-new}} = \sqrt{V_A^2 + \alpha + \beta} \quad (6)$$

$$V_{B\text{-new}} = \sqrt{V_B^2 - \alpha + \beta}. \quad (7)$$

Using these transforms, the fiber tip can be directed in any Cartesian direction from any starting point within the diamond alignment area. Starting in the middle of the actuator range, the fiber was actuated along trajectories every 45° for $|U| = 2000 \text{ V}^2$ and $|U| = 4000 \text{ V}^2$. The measured fiber locations after actuation are shown in Fig. 8. For the angled trajectories, one wedge remains stationary while the other wedge pushes the fiber up the slope, giving an angled trajectory. For the vertical and horizontal trajectories, the sloped wedges must move in tandem

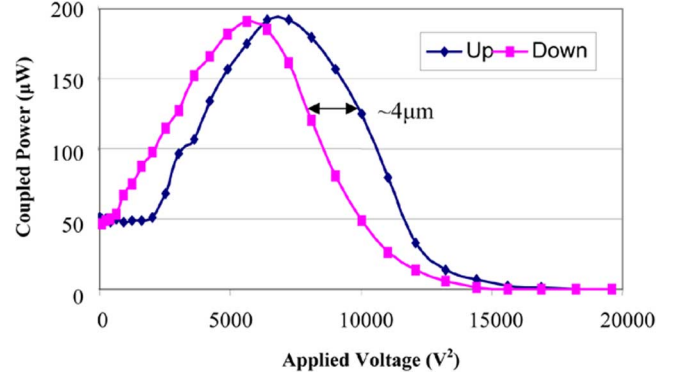


Fig. 9. Actuating both wedges with the same voltage creates a vertical up/down motion that exhibits significant hysteresis.

to produce the desired fiber movement. The slight nonlinearity over the $\sim 30\text{-}\mu\text{m}$ travel range is attributed to small asymmetries in wedge morphology and fiber rest position. However, these points clearly demonstrate that Cartesian control is possible.

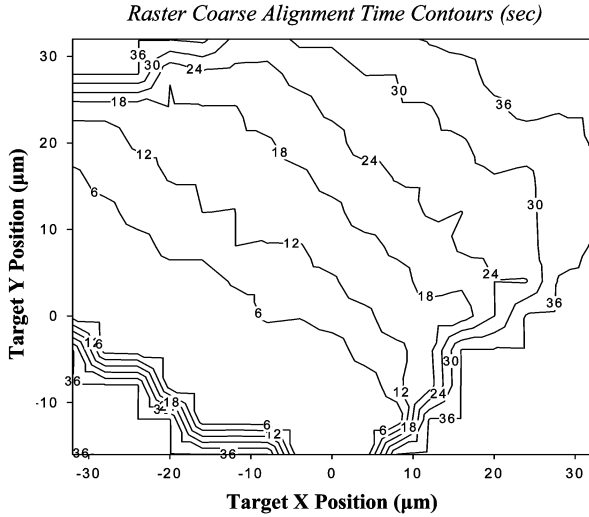
Another important characteristic to investigate is hysteresis of the fiber motion, primarily caused by the morphology of the grayscale wedges. To test the magnitude of this effect, the target fiber was fixed with a vertical offset compared to the grayscale fiber aligner. Thus, during a sequence of increasing then decreasing voltages, the grayscale fiber aligner tip passes through the point of peak coupling both on its way “up” and on its way back “down.” The coupled power between fibers was then measured as the grayscale fiber aligner actuated “up” and “down” over multiple cycles.

As shown in Fig. 9, there is the definite hysteresis between the “up” and “down” actuation paths. Using the calibrated electrostrictive stages to map the coupled power as a function of position, this “lag” is estimated to be equivalent to a shift of approximately $4 \mu\text{m}$ between the peaks. We believe this shift is caused primarily by frictional forces between the fiber and sloped wedges retarding the fiber motion along each trajectory. For displacements of at least a few microns, simple calculations show that the dominant mechanism determining the normal force between fiber and wedge (and, therefore, the frictional force) is the restoring spring of the fiber (rather than inertial forces). Thus, the friction is expected to increase slightly with fiber displacement as the bent fiber restoring force increases the normal force between fiber and wedge.

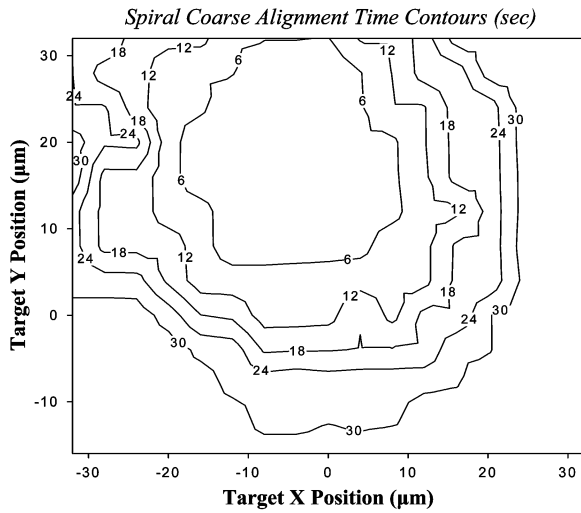
Hysteresis effects should be minimized, but not eliminated, by improving the wedge morphology through a combination of design and/or fabrication. However, fiber alignment using closed-loop control has proven robust with the current structures despite hysteresis effects. Single devices have also proven robust, in some instances actuating $> 10^5$ times in numerous testing configurations without any observed change in performance.

C. Automated Alignment—Speed

Most alignment algorithms start with a coarse alignment step to achieve an intermediate threshold power (to avoid noise and secondary peaks), before moving to a fine algorithm to finalize alignment. As shown experimentally later, the fundamental



(a)



(b)

Fig. 10. Coarse alignment time contours for different locations of the target fiber using (a) raster and (b) spiral algorithms [10].

choice and settings of each algorithm will have a significant effect on the speed with which final alignment is reached.

The simplest coarse alignment routine is that of a raster scan, where the voltage on the first actuator is held fixed, while the voltage on the second actuator is swept. The voltage on the first actuator is then incremented, and the sweep repeated. Fig. 10(a) shows the time required to achieve a coarse alignment threshold of 75% peak coupling, as a function of target fiber position. The sloped wedges cause the contour lines to be tilted with respect to the X - Y axes. Note that times > 36 s indicate failure to achieve threshold, loosely illustrating the diamond-shaped possible alignment area of this device. The primary drawback of a raster scan in a packaging application is that it begins searching for the peak in an unlikely position (the very edge of the travel range). For an optoelectronic module designed to rest in the center of the alignment area, it would take 12–18 s to achieve coarse alignment even if the fabrication and assembly were perfect.

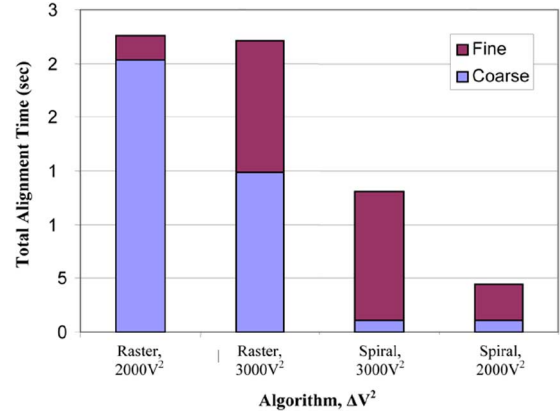


Fig. 11. Time to align within 95% peak power ($< 1.6 \mu\text{m}$) to a fixed InP waveguide, as a function of coarse search algorithm and Δ Voltage² setting.

To minimize coarse alignment time in this case, a spiral search algorithm was also developed and implemented for the grayscale fiber aligner to replace the raster scan. Rather than beginning at the edge like a raster scan, the spiral algorithm begins in the center of achievable motion, presumably the most likely location for the alignment target. The grayscale fiber aligner then proceeds to spiral outward to progressively less-likely positions until the coarse alignment threshold is reached. Fig. 10(b) shows the measured coarse alignment time for the same input fiber positions as before. For locations near the center, coarse alignment times < 6 s are achieved, confirming that the spiral algorithm is more efficient when the expected target location is near the center, as in a packaging application. It should be noted that the total time required to scan the entire alignment area was kept approximately the same (> 30 s) for both raster and spiral algorithms. While each algorithm uses different settings to define the scan mesh density, the primary difference between them is their start location. The implementation of these two basic algorithms, along with the Cartesian control possibilities discussed earlier, clearly demonstrate flexibility in controlling the grayscale fiber aligner using different methods.

To simulate in-package alignment of a III–V optical MEMS device, a $2\text{-}\mu\text{m}$ square InP suspended waveguide [16] was placed between the optical fibers. The waveguide was misaligned by approximately $\sim 20 \mu\text{m}$ with respect to the grayscale fiber aligner. The waveguide location was somewhere towards the middle of the aligner’s range, but the precise location was left unknown to simulate “blind” alignment. A hill-climbing algorithm [17] was modified to serve as the fine alignment step. The final alignment threshold was set to 95% of peak coupling, which corresponds to $1.6\text{-}\mu\text{m}$ misalignment (calibrated using the electrostrictive XYZ stages and measured Gaussian coupling profile).

Fig. 11 shows the total alignment time required using raster and spiral algorithms with different actuator step sizes (Δ Voltage² applied to comb drive). As expected for a quasi-centrally located target, the coarse alignment time dominates the total alignment time when using a raster algorithm,

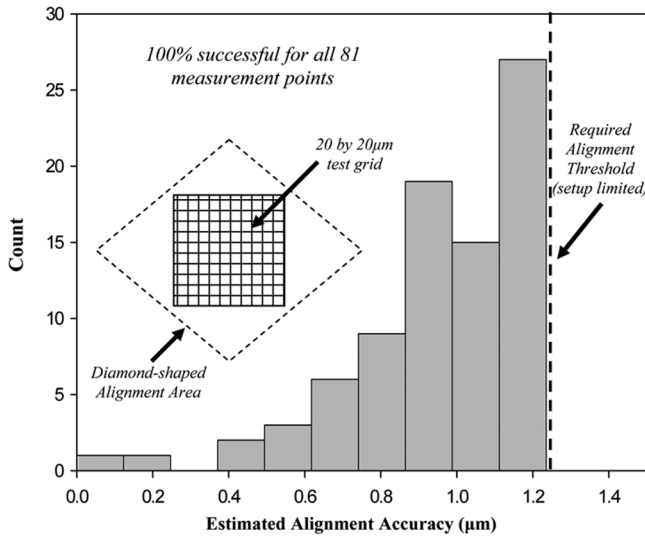


Fig. 12. Estimated alignment accuracy histogram for a 20-by-20- μm actuation area (with 2.5- μm grid), where alignment better than 1.25 μm (setup limited) was achieved with 100% success.

especially for smaller ΔV^2 (a finer scan mesh). Using the spiral algorithm dramatically decreased the coarse alignment time, but large ΔV^2 caused the fiber to temporarily overshoot the target location. The fastest alignment times were achieved using the spiral algorithm in conjunction with the smaller ΔV^2 .

While the exact time required to align to particular device will depend on its location, an accuracy of $< 1.6 \mu\text{m}$ was routinely achieved in 5–10 s to InP waveguides initially misaligned by $\sim 20 \mu\text{m}$. Additionally, many algorithm parameters can be adjusted to tailor the response speed and/or resolution for particular applications.

D. Automated Alignment—Accuracy

The previous experiments have established that high-accuracy alignment can be achieved quickly for a particular target location. However, the resolution achieved in the InP waveguide experiments could have been an artifact of the particular waveguide locations tested. Therefore, the InP waveguide was replaced with a lensed input fiber on the electrostrictive stage. This setup enables quick reconfiguration of target location (lensed fiber) to determine if high resolution can be achieved over the majority of the alignment area.

A 20-by-20- μm grid of target locations was selected within the diamond-shaped alignment area (shown in the inset of Fig. 12), with 2.5- μm spacing between points. For each position of the target fiber, the grayscale fiber aligner attempted to align within 95% peak coupling (1.25 μm accuracy when calibrated with electrostrictive stages). Initial results indicated success rates of approximately 70%, meaning the grayscale fiber aligner was not able to achieve the required alignment for 30% of the target locations (failed points were randomly scattered).

Upon further inspection, we realized the problem resided between our actuator and the traditional hill-climbing algorithm. Typically, hill-climbing algorithms step up a hill and after

passing the peak, turn around and scan again with a reduced step size. This process is repeated until sufficient alignment is reached (or the program gives up/times out). However, as the step size gets smaller for the grayscale fiber aligner, we observed that small changes in voltage no longer caused an appreciable movement, an effect we attribute to static friction between the wedges and fiber. Thus, depending on the fiber and target locations, as well as hysteresis effects and friction conditions, decisions within the algorithm were often based simply on noise fluctuations.

We chose to alter the fiber actuation scheme to include a 100-ms pulse of (0 V, 0 V) to “unstuck” and reset the fiber. This pulse also ensures a consistent starting point for actuation, which should reduce hysteresis effects. While the “pulse” method slows alignment slightly, it enables small ΔV^2 steps to create changes in fiber location. Alignment tests were performed over the same 20-by-20- μm area, but now using this “pulse” method of actuation in the fine alignment algorithm. As shown in the histogram of the estimated resolution in Fig. 12, the 1.25- μm required threshold was achieved with 100% success across the entire area (all 81 measured points). Most cases stopped after barely meeting this coupling threshold, but some exceeded it by a good amount, leading to the one-sided distribution of Fig. 12.

These results imply that continuous small displacements by the grayscale fiber aligner will be limited by the friction between the wedges and fiber. However, fibers can be positioned with accuracy below the minimum continuous movement threshold, as shown with the pulse actuation method.

V. DISCUSSION

While the fabrication and testing results presented here have demonstrated the capability of the grayscale fiber aligner, two primary areas for further development remain. First, improving the sloped wedge surface morphology could lead to more continuous movement and finer alignment accuracy. Redesign of the grayscale slope using more gray levels could minimize wedge roughness in photoresist at the expense of increasing optical mask cost. Techniques such as short isotropic silicon etching or hydrogen annealing [18] are candidates for postprocess smoothing of the surface, but would require careful process control to avoid effecting other geometries on the device.

Once acceptable coupling has been achieved by the grayscale fiber aligner, a constant application of voltage is required to maintain the alignment. Thus, the grayscale fiber aligner would benefit from the development of a mechanism for fixing the fiber in its final position, a necessary component of any fiber packaging scheme. There are two possible avenues to address this challenge. The first option is to immobilize the fiber via epoxy or soldering, which is typically a permanent process and may cause slight shifts in fiber position. Alternatively, a mechanical locking mechanism could be introduced to immobilize the silicon actuators themselves. MEMS bistable actuators [19] could be adapted to grip the comb-drive actuators to prevent any lateral movement of the wedges, holding them in their final aligned

positions. Thus, the deflected fiber restoring spring force ultimately holds the fiber at the bottom of this final v-groove to fix its position, where the total loss is a combination of residual axial misalignment and the small angular misalignment introduced by bending the fiber (see Section II). The primary advantage of a mechanical clamping approach is that the locking mechanism could be reversible, enabling repositioning of the fiber if any shifts occur during or after the clamping process. Significant design, simulation, and testing of such a mechanism would be required, with specific focus on the mechanisms susceptible to shock and/or vibration.

Calculations following the analysis presented in Section II and in [14] show that longitudinal alignment (along the axis of light propagation) is typically less sensitive than axial misalignment. Thus, combining our two-axes fiber actuator with passive techniques capable of coarse longitudinal alignment could provide three-axes alignment with limited changes to our design. However, extending our device to a 6 degree-of-freedom system (as desired in some applications) would be extremely difficult without significant increases in complexity and size, likely leading to a case of diminishing returns.

VI. CONCLUSION

The concept, design, fabrication, and testing of the grayscale fiber aligner clearly demonstrate its flexibility for aligning optical fibers in two axes. Actuation of a fiber cantilever $> 30 \mu\text{m}$ in both the horizontal and vertical axes is demonstrated, with an estimated resolution of $< 1.25 \mu\text{m}$ over much of the alignment area. The alignment times achieved with the on-chip grayscale fiber aligner compare favorably to active alignment times reported using external actuators [17]. The device configuration and control algorithms presented provide numerous avenues for optimizing active alignment time and accuracy for optoelectronics packaging. Alternative search algorithms could also be adapted to work with this device.

Future work will concentrate on improving wedge morphology and miniaturizing the actuator to enable alignment of fiber arrays in a compact footprint within optoelectronic packaging modules. Methods for further improving the alignment accuracy of grayscale fiber aligners will also be pursued, in conjunction with investigations into securing the fiber in its final location.

ACKNOWLEDGMENT

The authors would like to thank the staff of the Army Research Lab (ARL) and the Laboratory for Physical Sciences (LPS) for access to their cleanroom facilities, and Northrop Grumman for optical mask fabrication.

REFERENCES

- [1] C. A. Armiento, A. J. Negri, M. J. Tabasky, R. A. Boudreau, M. A. Rothman, T. W. Fitzgerald, and P. O. Haugsjaa, "Gigabit transmitter array modules on silicon waferboard," *IEEE Trans. Compon., Hybrids, Manuf. Technol.*, vol. 15, no. 6, pp. 1072–1080, Dec. 1992.

- [2] P. Schwab, T. Bowen, R. Perko, N. Delen, J. Goodrich, and R. Anderson, "A high throughput optoelectronic module assembly process," in *Proc. 54th Electron. Compon. Technol. Conf.*, 2004, vol. 2, pp. 1475–1478.
- [3] W. J. Shakespeare, R. A. Pearson, J. L. Grenestedt, P. Hutapea, and V. Gupta, "MEMS integrated submount alignment for optoelectronics," *J. Lightw. Technol.*, vol. 23, no. 2, pp. 504–509, Feb. 2005.
- [4] J. M. Haake, R. L. Wood, and V. R. Dhuler, "In-package active fiber optic micro-aligner," in *Proc. SPIE—Int. Soc. Opt. Eng.*, 1998, vol. 3276, pp. 207–219.
- [5] T. Frank, "Development and manufacturing of a two-dimensional microactuator for moving of an optical fibre," in *Proc. SPIE—Int. Soc. Opt. Eng.*, 1996, vol. 2882, pp. 238–246.
- [6] C. M. Waits, A. Modafe, and R. Ghodssi, "Investigation of gray-scale technology for large area 3D silicon MEMS structures," *J. Micromech. Microeng.*, vol. 13, pp. 170–177, 2003.
- [7] B. Morgan, C. M. Waits, J. Krizmanic, and R. Ghodssi, "Development of a deep silicon phase Fresnel lens using gray-scale lithography and deep reactive ion etching," *J. Microelectromech. Syst.*, vol. 13, no. 1, pp. 113–120, Feb. 2004.
- [8] C. M. Waits, B. Morgan, M. Kastantin, and R. Ghodssi, "Microfabrication of 3D silicon MEMS structures using gray-scale lithography and deep reactive ion etching," *Sens. Actuators A, Phys.*, vol. 119, pp. 245–253, 2005.
- [9] B. Morgan and R. Ghodssi, "On-chip 2-axis optical fiber actuator using gray-scale technology," in *Proc. IEEE MEMS*, Istanbul, Turkey, 2006, pp. 266–269.
- [10] —, "Automated optical fiber alignment in 2-axes using 3-D shaped actuators," in *Proc. Solid State Sens., Actuator, Microsyst. Workshop*, Hilton Head Island, SC, Jun. 4–8, 2006, pp. 70–73.
- [11] C. Sy-Hann, L. Heh-Nan, and O. Pang-Ming, "Spring constant measurement of a bent near-field optical fiber probe," *Rev. Sci. Instrum.*, vol. 71, pp. 3788–3790, 2000.
- [12] R. Legtenberg, A. W. Groeneveld, and M. Elwenspoek, "Comb-drive actuators for large displacements," *J. Micromech. Microeng.*, vol. 6, pp. 320–329, 1996.
- [13] J. M. Maloney, D. S. Schreiber, and D. L. DeVoe, "Large-force electrothermal linear micromotors," *J. Micromech. Microeng.*, vol. 14, pp. 226–234, 2004.
- [14] D. Marcuse, "Loss analysis of a single-mode fiber splice," *Bell Syst. Tech. J.*, vol. 56, pp. 703–718, 1977.
- [15] B. Morgan and R. Ghodssi, "Design and simulation of comb-drive actuators incorporating gray-scale technology for tailored actuation characteristics," presented at the SPIE Microtechnol. New Millennium, Seville, Spain, May 9–11, 2005.
- [16] D. P. Kelly, M. W. Pruessner, K. Amarnath, M. Datta, S. Kanakaraju, L. C. Calhoun, and R. Ghodssi, "Monolithic suspended optical waveguides for InP MEMS," *IEEE Photon. Technol. Lett.*, vol. 16, no. 5, pp. 1298–1300, May 2004.
- [17] J. Guo and R. Heyler, "Fast active alignment in photonics device packaging," in *Proc. 54th Electron. Compon. Technol. Conf.*, 2004, vol. 1, pp. 813–817.
- [18] M.-C. M. Lee and M. C. Wu, "3D silicon transformation using hydrogen annealing," in *Proc Solid-State Sens., Actuator, Microsyst. Workshop*, Hilton Head Island, SC, 2004, pp. 19–22.
- [19] H. N. Kwon, H. Il-Han, and L. Jong-Hyun, "A pulse-operating electrostatic microactuator for bi-stable latching," *J. Micromech. Microeng.*, vol. 15, pp. 1511–1511, 2005.



Brian Morgan (S'01–M'02) received the B.S. degree in physics from Georgetown University, Washington, DC, in 2002 and the M.S. and Ph.D. degrees in electrical engineering from the University of Maryland, College Park, in 2004 and 2006, respectively.

He received graduate research support through multiple fellowship awards, including an ARL fellowship. He joined the Sensors and Electron Device Directorate (SEDD) at the U.S. Army Research Laboratory (ARL) in Adelphi, MD, as an

Electronics Engineer in Fall 2006. His main research interests are in the areas of electrostatic MEMS devices and 3-D fabrication technologies.

Dr. Morgan is the member of Sigma Xi Scientific Research Society and the recipient of the Achievement Rewards for College Scientists (ARCS) Fellowship (Metropolitan Washington Chapter) for 2004–2005 and 2005–2006.



Jonathan McGee (S'05) received the B.S. degree in electrical engineering from the University of Maryland, College Park, in 2004, where he is currently working towards the M.S. and Ph.D. degrees in electrical engineering.

His main research interests are in the area of optical MEMS devices. He is a student member of American Vacuum Society (AVS).



Reza Ghodssi (M'92) received the B.S., M.S., and Ph.D. degrees in electrical engineering from the University of Wisconsin at Madison, in 1990, 1992, and 1996, respectively.

He is an Associate Professor in the Department of Electrical and Computer Engineering and the Institute for Systems Research (ISR) at the University of Maryland (UMD), College Park. He is also the Director of the MEMS Sensors and Actuators Lab (MSAL) at the UMD and a core faculty member in the Bioengineering Graduate Program and the Maryland NanoCenter at UMD. He was a Postdoctoral Associate and a Research Scientist in the Microsystems Technology Laboratories and the Gas Turbine Laboratory at the Massachusetts Institute of Technology (MIT), Cambridge, from 1997 until 1999. He has over 50 scholarly publications. He is the Co-Founder of the MEMS Alliance in the greater Washington area. His research interests are in the design and development of microfabrication technologies and their applications to microsensors, microactuators, and integrative microsystems for biosensing, powerMEMS, and energy harvesting.

Dr. Ghodssi is a member of the American Vacuum Society (AVS), the Materials Research Society (MRS), the American Society for Engineering Education (ASEE), and the American Association for the Advancement of Science (AAAS). He received the 2001 UMD George Corcoran Award, the 2002 National Science Foundation CAREER Award, and the 2003 UMD Outstanding Systems Engineering Faculty Award. He has served as a Program Co-Chairman for the 2001 International Semiconductor Device Research Symposium (ISDRS) and as a Chairman of the "MEMS and NEMS Technical Group" at the AVS from 2002 to 2004.